



**HAL**  
open science

## Multiscale identification of the inorganic shell of core (Co)/shell-assembled nanoparticles

Ghilhem Simon, Salvatore Costanzo, Isabelle Lisiecki, Philippe Colombari

► **To cite this version:**

Ghilhem Simon, Salvatore Costanzo, Isabelle Lisiecki, Philippe Colombari. Multiscale identification of the inorganic shell of core (Co)/shell-assembled nanoparticles. *Journal of Raman Spectroscopy*, 2024, 55, 10.1002/jrs.6668 . hal-04496649

**HAL Id: hal-04496649**

**<https://hal.science/hal-04496649>**

Submitted on 8 Mar 2024

**HAL** is a multi-disciplinary open access archive for the deposit and dissemination of scientific research documents, whether they are published or not. The documents may come from teaching and research institutions in France or abroad, or from public or private research centers.

L'archive ouverte pluridisciplinaire **HAL**, est destinée au dépôt et à la diffusion de documents scientifiques de niveau recherche, publiés ou non, émanant des établissements d'enseignement et de recherche français ou étrangers, des laboratoires publics ou privés.

# Multiscale identification of the inorganic shell of core (Co)/shell-assembled nanoparticles

Ghilhem Simon  | Salvatore Costanzo  | Isabelle Lisiecki  |  
Philippe Colombar 

Sorbonne Université, CNRS, MONARIS,  
UMR8233, Paris, France

## Correspondence

Philippe Colombar, Sorbonne Université,  
CNRS, MONARIS, UMR8233, Paris  
F-75005, France.  
Email: [philippe.colombar@sorbonne-universite.fr](mailto:philippe.colombar@sorbonne-universite.fr)

## Abstract

Core (Co)/shell (Co-oxide) nanoparticles assembly exhibits interesting magnetic properties that depend on the inorganic shell characteristic (composition and crystalline structure). Assemblies of pure and partially oxidized cobalt (core/shell) nanoparticles, ~9 nm in diameter, were prepared and analyzed by techniques probing the matter at macroscale to nanoscale: UV-visible-near-infrared (NIR) transmission, FTIR, Raman microspectroscopy, and transmission electron microscopy. Attention is paid to compare nonoxidized and (partially) oxidized Co nanoparticles, coated with lauric acid as stabilizing agent (ligands). The approximately 1 nm disordered inorganic coating is perfectly detected by transmission electron microscopy, UV-visible-NIR, infrared, and Raman spectroscopy. The Raman spectrum is sensitive to laser wavelength and power due to the local heating induced by the laser, which modifies the interaction between the organic chains and the nanoparticle inorganic shell. For comparison, nanoparticle films were analyzed under heating from room temperature to 300°C. The “fusion” (dynamic disorder) of lauric (dodecanoic) chains is observed concomitantly with the merging of very low wavenumber Lambs’ modes into a Rayleigh wing, which is consistent with an increase in the topological nanoparticle disorder. Hydroxylation or water adsorption is observed for Co film. The UV-visible-NIR and Raman spectra of the Co-oxide shell do not correspond to that of CoO (rock salt) nor to that of Co<sub>3</sub>O<sub>4</sub> (spinel) but has some similarity to that of 2D delafossite (CoOOH) phase.

## KEYWORDS

cobalt, cobalt oxide, core/shell, delafossite, nanoparticles

## 1 | INTRODUCTION

The attention paid to the study of assemblies of nanoparticles (NPs), formerly called colloids, has been growing

since the seminal review paper of Matijevic in the 1980s<sup>1</sup> and the merging of the development of sol-gel techniques initiated in the 1960s.<sup>2,3</sup> If at the beginning, main of the NPs were oxides, then since a long time, most of

This is an open access article under the terms of the [Creative Commons Attribution-NonCommercial-NoDerivs](https://creativecommons.org/licenses/by-nc-nd/4.0/) License, which permits use and distribution in any medium, provided the original work is properly cited, the use is non-commercial and no modifications or adaptations are made.

© 2024 The Authors. *Journal of Raman Spectroscopy* published by John Wiley & Sons Ltd.

the works are focused on nonoxidizable or poorly oxidizable metallic NPs (i.e. metals found naturally in the native state: gold, silver, and copper).<sup>4–8</sup> It is only in recent years that researchers have focused on more reactive metals such as cobalt.<sup>9–15</sup> It is obvious that the fields of application of NPs, effective or potential, were and remain very varied: oxide or metallic materials (and their precursors) for optical (synthetic gems, ceramics, and optics), thermo-mechanical (nanocomposites), elect(ochem)ical (electrodes), catalysis (particles), and magnetic application (memory).<sup>1,2,16–32</sup> Depending on the desirable properties, the NPs must be single component, that is, pure metallic or oxide, or multicomponent as this is the case for the core/shell geometry, characterized for instance by a metallic core and an oxidized shell NPs.<sup>20,22,33,34</sup> In a general way, the small size of the objects maximizes the proportion of atoms at the surface and the curvature of the surface promotes the defect rate and the chemical reactivity of the particles.<sup>35</sup>

Agglomeration and coalescence between the NPs take place at low temperature, which is desired for certain applications such as the low-temperature sintering/densification,<sup>2,3</sup> but have a damaging effect for many others; this is the case for porosity control, magnetic properties, reactivity, electrochemical stability, and so forth of metal particles.<sup>36</sup> To keep the integrity of the NP, organic molecules are used as protective coating, which strongly interact with the NP surface. These latter, also called stabilizers or ligands, allow to control particle–particle interactions and thus their assembly,<sup>37,38</sup> to obtain more or less ordered single-layer (2D) or multi-layer films (3D) for even well-shaped supercrystals (adjacent or isolated ones, also called colloidal crystals) formed by 3D ordering of NPs.<sup>39–42</sup> The head of these ligands, which bind to the NP surface, is generally sulfided or carboxylated and the body is a fatty acid chain.<sup>12,42</sup> These compounds are also called “metal soaps” having long been known for the protection of metals.<sup>43</sup>

As shown by the reviews written in the 1990s,<sup>1,2</sup> the synthesis of monodispersed NPs is old but large-scale development is now linked to the easier possibilities of visualization (SEM, transmission electron microscopy [TEM], and AFM microscopy) and of measurements of properties at micron and submicron scales.<sup>44–48</sup> Optical spectroscopy and, in particular, Raman analysis make it possible, via the analysis of the modes of vibration of the particles themselves (Lamb modes),<sup>49–53</sup> to obtain information on certain physical properties of the matter constituting the single particle. The demonstration of the easy synthesis of silver NP aggregates by Creighton et al. in 1979<sup>54</sup> led to a great development of the Raman SERS analysis discovered more than 40 years ago independently by Fleischmann et al.<sup>55</sup> and Jeanmaire and Van Duyne<sup>56</sup>

but characterization of the NPs, and especially of their “surface,” using vibrational spectroscopy remains long times limited.<sup>57,58</sup> The attention paid to the identification by vibration—infrared and/or Raman spectroscopy—of the organic phase constituting the assemblies of NPs received considerable attention<sup>30,34,59,60</sup> but does not concern the skin of (metal)/shell (metal oxide) systems. Attention has also concerned the phenomena of Raman exhalation.<sup>61–63</sup> Here, we present the first combined TEM, UV–visible, Raman, and FTIR analysis of assemblies of core (Co)/shell (Co oxide) NPs dedicated to the characterization of the inorganic shell probed at different scales.

## 2 | EXPERIMENTAL

### 2.1 | Synthesis

#### 2.1.1 | Products

All materials were used as received without further purification: Cobalt acetate, lauric (dodecanoic) acid, sodium borohydride, and octylether are from Aldrich, isooctane and hexane from Fluka, and sodium di (ethylhexyl) sulfosuccinate (NaAOT) from Sigma. The synthesis of cobalt (II) bis(2-ethylhexyl) sulfosuccinate (Co (AOT)<sub>2</sub>) was described previously.<sup>64</sup> CoO and Co<sub>3</sub>O<sub>4</sub> powders were provided from Sigma-Aldrich.

#### 2.1.2 | Co NPs

Co NPs stabilized by lauric acid chains are synthesized via chemical reduction in reverse micelles as described in previous papers.<sup>12,64–66</sup> By controlling the reducing agent (sodium borohydride) concentration, a narrow size distribution of Co NPs is obtained. The entire synthesis is carried out in a N<sub>2</sub> atmosphere dry glove box using deoxygenated solvents to prevent uncontrolled Co oxidation. The NPs are dispersed in hexane.

#### 2.1.3 | Co@Co-oxide NPs

The oxidation process is conducted in hexane. A colloidal solution of Co NPs passivated with lauric acid is prepared with a concentration of 8 10<sup>−3</sup> M NPs and transferred to a beaker. The solution is first subjected to air bubbling for 2 min, and then, the beaker is sealed and left at room temperature for 12 days in order to allow a slow oxidation of Co metal from the oxygen retained by the solution. NP film is then deposited on the different substrates selected to fit with the analytical technique.

## 2.2 | Methods and sample preparations

### 2.2.1 | Transmission electron microscopy

TEM study is performed using a JEOL JEM-1011 microscope at 100 kV. For this study, samples are prepared by depositing some drops of the Co and Co@oxide NP solution on a Cu grid covered with a carbon thin film.

### 2.2.2 | Profiles and histograms

The histograms of the NPs are obtained by measuring their diameter  $D_i$  of at least 500 NPs deposited on a TEM copper grid. The standard deviation,  $\sigma$ , is calculated from the experimentally determined distribution using the formula.

$$\sigma = \left\{ \left[ \sum ni (Di - D)^2 \right] / [n - 1] \right\}^{1/2},$$

where  $n$  is the number of NPs measured and  $D$  to the average diameter.<sup>50</sup>

### 2.2.3 | UV–visible–NIR absorption spectra

UV–visible–near-infrared (NIR) absorption spectra are recorded on a conventional Cary 5000 Varian spectrophotometer. Acquisitions are carried out with colloidal solutions of NPs dispersed in hexane on a Suprasil<sup>®</sup> UV-transparent silica plate made hydrophobic by a 10 nm layer of amorphous carbon. The surface analyzed is several tens of square millimeters, the distribution of the sample deposit being fragmentary (not continuous). NP layer is then exposed to air. Analyses are carried out 24 h after preparation.

### 2.2.4 | Raman microspectroscopy

Raman measurements are performed using LabRam HR800 setup (Horiba, Jobin Yvon, France), equipped with an Ar<sup>+</sup> ion plasma laser Innova I90C 6UV (Coherent Inc., Santa Clara, CA, USA) allowing multiple wavelengths from ultraviolet to red light. Working with 514.5 nm laser excitation and equipped with BragGrate<sup>®</sup> notch filters from Optigrate (Oviedo, FL, USA) Stokes and anti-Stokes spectra are recorded up to the Rayleigh peak, that is, down to  $\sim 4 \text{ cm}^{-1}$ . Spectral resolution with 1800 and 600 lines per millimeter gratings are about 0.5 and  $3 \text{ cm}^{-1}$ , respectively. Blue (457 nm) and red (633 nm) laser lines are also used but recorded with a limited

low-wavenumber spectral range (cut-off at  $\sim 60$  and  $30 \text{ cm}^{-1}$ , respectively). Thick assemblies of Co and Co@oxide NPs are prepared by horizontally immersing HOPG substrates (10 mm  $\times$  5 mm) in 200  $\mu\text{L}$  of  $5.5 \times 10^{-7} \text{ M}$  colloidal NP solution. The solvent evaporation takes place at  $35^\circ\text{C}$  under nitrogen flow. Deposits on a glass plate covered by a gold layer are also analyzed. With the used optics (ULWD Olympus 100 $\times$  and ULWD Mitutoyo 200 $\times$  microscope objectives, numerical aperture of 0.80 and 0.62, respectively), the surface of the laser spots is less than  $3 \times 3$  and  $1 \times 1 \mu\text{m}^2$ . Analyses are carried out in air 24 h after preparation. We will discuss the in-depth penetration of the light and the volume of matter probed by Raman microscopy further. CoO and Co<sub>3</sub>O<sub>4</sub> powders have been analyzed and deposited on a glass plate coated with an opaque gold film. Attention was paid to use very low illumination power (down to 50  $\mu\text{W}$ ).

A Linkam heating cell (Oxford) is used to record spectra at different temperatures.

### 2.2.5 | Infrared spectroscopy

Infrared measurements are performed by using an Equinox spectrometer (Bruker Optics, Ettlingen, Germany) using transmission mode. Infrared samples are prepared by depositing a few drops of Co and Co@oxide NPs dispersed in hexane on CaF<sub>2</sub>, CsI, and KRS5<sup>®</sup> single crystal wafer in dry glove box. After a complete evaporation of the hexane in the glove box, a second wafer is used to cover the first one and the two wafers are placed in a cell for solid examination<sup>67</sup> with polymer rings in order to protect the sample from the ambient air. Removal of the top wafer exposes the NP layer to ambient air.

## 3 | RESULTS AND DISCUSSION

### 3.1 | Topology and structure of pure Co NPs and partially oxidized Co NPs

Figure 1 compares the topology and structure of pure Co NPs with those of partially oxidized Co NPs obtained after the oxidation for 12 days. As shown in the TEM image (Figure 1A), lauric acid-coated Co NPs deposited on a TEM grid are characterized by a mean diameter of 8.7 nm (histograms are given in Figure S1). Due to their low size distribution (10%), they self-organize in 2D or thin 3D superlattices (Figure 1B).<sup>65</sup> Previous study shows that they are poorly crystallized in a face-centered cubic (fcc) structure.<sup>53</sup>

After their oxidation in hexane and their deposition on a TEM grid, the TEM images obtained in medium and

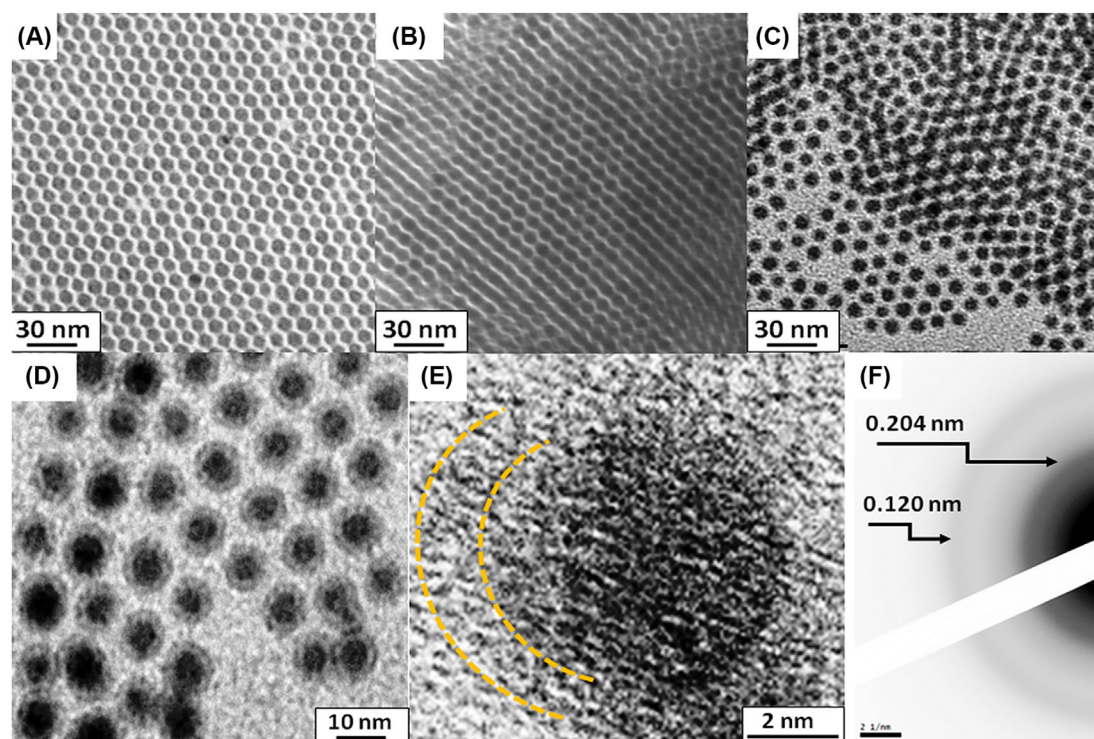


**FIGURE 1** Transmission electron microscopy images of assemblies of as-synthesized cobalt nanoparticles (A, single layer; B, multilayer) and core (Co)/shell (Co oxide) nanoparticles (C, single/bilayer, and D, single layer), after their partial oxidation. (E) High-resolution transmission electron microscopy image of one single core (Co)/shell (Co oxide) nanoparticle with delimitation of the “oxidized” shell. (F) Electron diffraction pattern made over the region shown in (C).

high resolutions (Figure 1C–E) show a rather well-contrasted core/shell structure. The average Co core diameter and “oxide” shell thickness of sample used for TEM are found equal to 5.6 and 0.85 nm, respectively, which, in turn, give rise to a total diameter of  $0.85 + 5.6 + 0.85 = 8.7$  nm, that is, the diameter of pristine pure Co NPs. As for Co NPs, these NPs tend to self-organize in 2D and thin 3D superlattices. However, due to their poorer size distribution (16% instead of 10% for Co NPs; Figure S1), these superlattices are characterized by a lower coherence length compared with those made of nonoxidized Co NPs (Figure 1C,D).

The high-resolution TEM does not reveal any lattice planes in both the core and the shell of the NPs indicating poor crystallinity. However, the electron diffraction pattern (Figure 1F) shows two diffuse diffraction rings at 0.204 and 0.124 nm, which are indexed as the (111) and (220) spacing of fcc cobalt. On one hand, this result further confirms the low crystallinity of the metallic fcc core. On the other hand, we do not detect any signature of the cobalt oxide shell. This last feature is attributed both to the very low crystallinity of the shell material and to the low amount of this material.

It is noticeable that these partially oxidized NPs are highly stable (in air and in vacuum) and do not coalesce, even under examination in the microscope (Figure 1C,D).

### 3.2 | Representativeness of the measurement with different techniques

The analysis methods do not see matter according to the same criteria and above all the surfaces of matter and the depth explored are very different, a few thousand square nanometers for TEM, a few to a few tens of square micrometers in Raman microspectroscopy, and a few hundreds to thousands of square millimeters in infrared and UV–visible–NIR spectroscopy.

It is not possible to perform TEM and vibrational analysis on the same area on a sample, and in any case, the surface analyzed by optical spectroscopy (Raman, infrared, and UV–visible spectroscopy) is several orders of magnitude larger than that visualized in TEM. Therefore, topographic TEM analysis should be considered only as an illustration of the topology of the samples analyzed by optical spectroscopy. Direct topological analysis

in TEM measuring the diameter of the NPs (Figure 1) and the calculation of the diameters of the NPs from the law relating the wavenumber of the main mode of Lamb<sup>49,52,53</sup> measured by Raman microscopy must lead to the same value if the local topology (TEM) is representative.

Figure 2 compares the spectra obtained at low wavenumbers for Co and core (Co)/shell (Co-oxide) NPs. The relationship previously established for Co NPs<sup>53</sup> allows us to calculate the mean particle diameter from the Raman wavenumber of the main Lamb mode (quadrupole vibration): The Raman analysis is carried out on a much larger area ( $\times 100$  microscope objective, i.e.  $< \sim 10 \mu\text{m}^2$ ) than that of the TEM analysis. Using the correlation established for the pure cobalt NPs<sup>53</sup> and applying it to the core/shell NPs gives an estimate of the average diameter. This value is consistent with that measured directly at the local scale from the TEM images (8.7 nm). This means that the shell does not significantly change the mechanical constant of the NP. The poorer definition of the size of metallic cores may explain the expansion of quadrupole Raman ( $\sim 10 \text{ cm}^{-1}$ ) and breathing ( $\sim 20 \text{ cm}^{-1}$ ) modes. The two quadrupole mode wavenumbers measured are  $\sim 9$  and  $8 \text{ cm}^{-1}$  for oxidized and pure cobalt NPs, respectively (the surface area analyzed is less than  $10 \mu\text{m}^2$ ), which, according to the relationship of Figure 2B, corresponds to 6 and 9 nm to be compared with the value of 8.7 nm measured by TEM at shorter

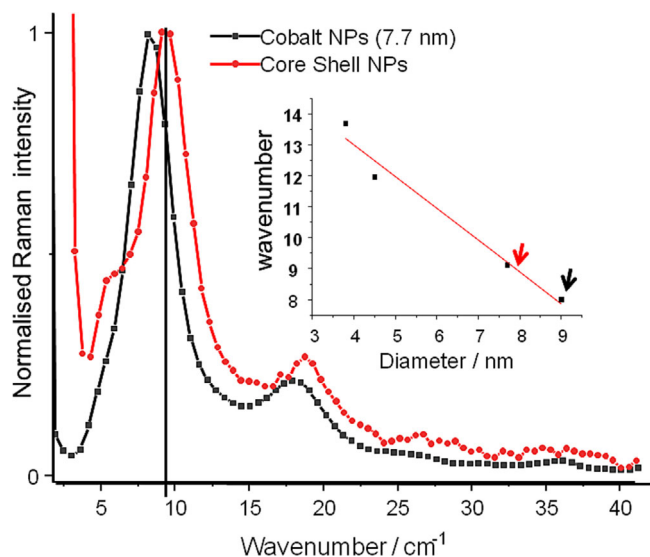


**FIGURE 2** Comparison of Lamb modes for assemblies of pure Co nanoparticles and core (Co)/shell (Co-oxide) (Co@CoO) nanoparticles at RT; (Insert) the wavenumber makes it possible to calculate the average diameter from the correlation  $d = f$  [wavenumber] (after the literature<sup>53</sup>). Arrows indicate corresponding wavenumber and nanoparticle (NP) diameter on the relationship.

scale ( $\sim 5 \cdot 10^{-2} \mu\text{m}^2$ ). Results are consistent. With both methods, the thickness of the oxide shell is  $\sim 1 \text{ nm}$  that corresponds to two or three layers of cobalt-oxygen bond. We can thus expect that TEM images are also representative of the sample studied by UV-visible-NIR absorption while the number of NPs analyzed is much larger.

### 3.3 | Macroscopic characterization: UV-visible transmission

Figure 3 compares the UV-visible-NIR absorption spectra recorded on the deposit of “pure” Co NPs and of partially oxidized Co NPs. Absorption profiles are different. The subtracted spectrum shows significant absorption from  $\sim 600$  to  $680 \text{ nm}$  as well as possible components around 270, 360, 460, 510, and beyond  $800 \text{ nm}$ . However, the characterizations of  $\text{Co}^{2+}$  and  $\text{Co}^{3+}$  ions in vitreous silicate matrices and in aluminosilicate crystalline phases show absorptions at 524, 596, and  $650 \text{ nm}$  ( $\text{Co}^{2+}$ ,

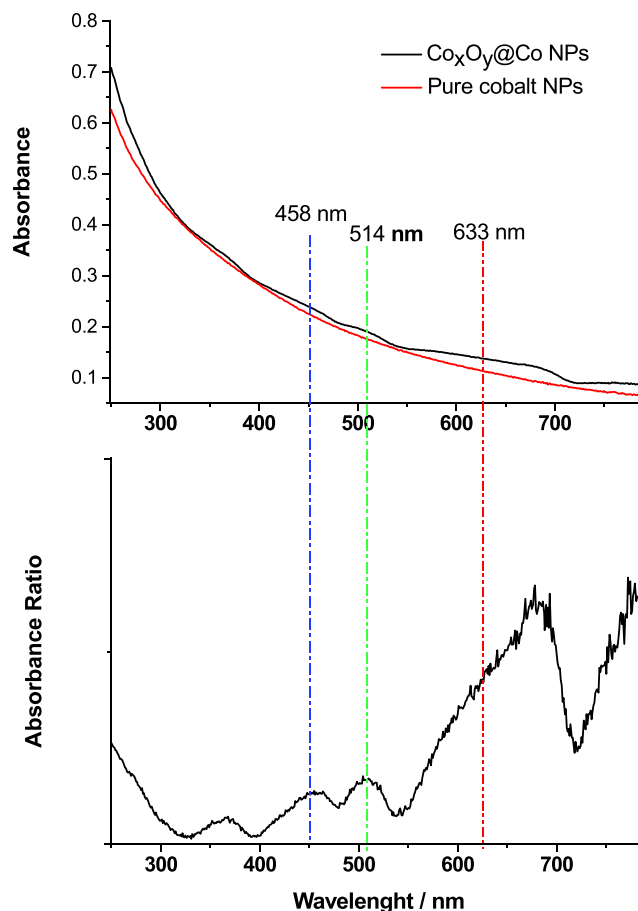


**FIGURE 3** Comparison of optical absorptions measured for silica deposition of pure Co nanoparticle (NP) and core (Co)/shell NP assembly (top); (bottom) difference spectrum. The wavelengths of the lasers used for Raman analysis are indicated.

tetrahedral site) and 270, 344, 470, 506, 544, 600, 636, 644, and 1196 nm ( $\text{Co}^{3+}$ , octahedral site).<sup>68–71</sup> The spectra are therefore compatible with the existence of both types of ions but the components assigned to  $\text{Co}^{2+}$  seem dominant, if we except the likely absorption above 800 nm.

### 3.4 | Characterization of organic ligand spacers

Figure 4A compares the infrared spectra obtained for layers of nonoxidized and partially “oxidized” particles deposited on a CsI crystal wafer and protected from the air by a second CsI wafer. The comparison is made with the spectrum of lauric acid ( $\text{CH}_3-(\text{CH}_2)_{10}-\text{COOH}$ ). Raman spectra are shown in Figure 3B. We will first consider infrared signatures.

#### 3.4.1 | Infrared signatures

For each compound, a very specific spectrum is observed. Only the thin bands of the  $2800\text{--}3100\text{ cm}^{-1}$  region, characteristic of the C–H stretching of the  $\text{CH}_3$  and  $\text{CH}_2$  groups, appear to be roughly preserved, indicating the conservation of (some of) the  $\text{CH}_3-(\text{CH}_2)_{10}$  chains. Tables 1 (infrared) and 2 (Raman) show the wavenumbers of the different bands.

The disappearance of the broad band between  $2500$  and  $3100\text{ cm}^{-1}$  characteristic of the hydrogen bond of the lauric acid proves the formation of a salt in accordance with its interaction with surface of the metal NPs. The

infrared spectra of the films of pure cobalt and “oxidized” cobalt NPs are very different: The Co NP film shows a broad band at  $3430$  with a shoulder at  $3100\text{ cm}^{-1}$  typical of traces of adsorbed water molecules and/or hydroxyl ions<sup>72</sup> and a spectrum complex, formed of intense broad features below  $1700\text{ cm}^{-1}$ , rather similar to that observed for conducting polymers with a metallic character.<sup>73,74</sup> The formation of the thin “oxide” shell therefore strongly modifies the infrared signature according to the huge variation of optical properties between an insulator or semiconductor (oxide phase) and a metal. Consequently, the complex infrared feature peaking at  $1583\text{ cm}^{-1}$  can be a reflection peak due to expected light reflection at a metal/oxide interface<sup>73,74</sup>; in that case, due to the theoretical shape of a reflection peak, the wavenumber to be considered is the inflexion point, at about  $1630\text{ cm}^{-1}$ . In that case, this is consistent with the assignment to the water molecule bending mode, counterpart of the  $\sim 3400\text{ cm}^{-1}$  broad band characteristic of water molecules.<sup>72</sup> However, it is not possible to know if the water is embedded between the ligands or hydrogen bonded to the metal surface.

On the contrary, the infrared spectrum obtained for the film of partially “oxidized” Co NPs shows well-defined bands, but at positions a little different from those of the acid. The intense C=O band observed at  $\sim 1700\text{ cm}^{-1}$  in pristine lauric acid, characteristic of the –COOH group, is observed only at very low intensity for the “oxidized” NP film. The disappearance of this band has already been observed by Ledo-Suarez et al.<sup>39</sup> for cobalt NPs dispersed in a KBr pellet and is considered as a proof of the grafting on metal particles. Ledo-Suarez et al.<sup>39</sup> assigned the shift of  $\text{CH}_2$  stretching mode from

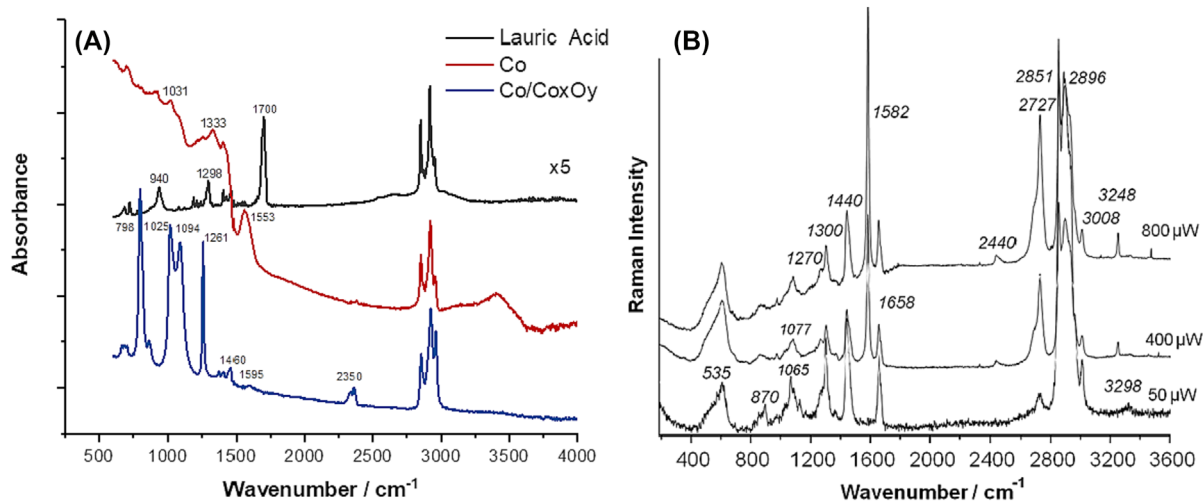


FIGURE 4 (A) Comparison of FTIR spectra of lauric acid film (lauric acid, intensity  $\times 5$ ), pure cobalt nanoparticles (Co), and core (Co)/shell (Co-oxide) (Co/Co<sub>x</sub>O<sub>y</sub>) nanoparticles. The wavenumbers of the main bands are given in Table 1. (B) Effect of laser illumination power (514.5 nm and 50, 400, and 800  $\mu\text{W}$ ) and induced heating on Raman spectra of core (Co)/shell (Co-oxide) nanoparticles deposited on HOPG.

**TABLE 1** Infrared modes ( $\text{cm}^{-1}$ ) recorded for lauric (dodecanoic) acid, Co nanoparticles (Co NPs), and core (Co)/shell (Co@Co-oxide) nanoparticles.

Mode/compound	Oleate	$\delta\text{H}_2\text{O}$	$\nu\text{C}=\text{O}$	$\nu\text{sCH}_n$	$\nu\text{asCH}_n$	$\nu\text{O-H}$	$\nu\text{H}_2\text{O}$	$\delta\text{H}_2\text{O}$			
Lauric acid	no	no	1699 vS	2850 S	2871 w	2917 vS 2952 w	3005 w	2500–3200 bw no	no		
Co NPs	1556 Sb	1630	no	2852 m	2865 w	2921 m 2956 w	no	no	3430 mb 1630		
Co@oxide NPs	no	1595 vw	1700 vw	2854 m	no	2923 m 2962 m	no	no	no	no	
Mode/Compound	$\nu\text{C-O}, \delta\text{CH}_n, \text{etc.}$										
Lauric acid	750 w	939 m	no	no	no	1348 m	no	1410 w	1431 w	1469 m	
Co NPs	805 w	920 w	1025 w	no	no	1390 m	no	no	no	1450 w	
Co@oxide NPs	798 vS	no	1020 S	1093 S	1261 S	no	1378 vw	1412 vw	1440 vw	1463 w	

Abbreviations: b, broad; m, medium; no, not observed; S, strong; v, very; w, weak.

**TABLE 2** Raman mode wavenumbers of cobalt oxides and Co@shell (in bold).

Laser wavelength	457 nm	514 nm	632 nm	Assignments
	195 w,n	224		$\text{Co}_3\text{O}_4$ ( $\text{F}_{2g}$ )
	476 w,n	482 w,n	489 S,n	$\text{Co}_3\text{O}_4$ ( $\text{E}_g$ )
	<b>486 w,b</b>			<b>Shell</b>
	516 w,n	522 w,n	515 w,n	$\text{Co}_3\text{O}_4$ ( $\text{F}_{2g}$ )
		530 w,b		
	<b>598 m,b</b>	<b>602 m,b</b>		<b>Shell</b>
	615 w,n		615 w,n	$\text{Co}_3\text{O}_4$ ( $\text{F}_{2g}$ )
	685 S,n	691 s,n	691 w,n	$\text{Co}_3\text{O}_4$ ( $\text{A}_{1g}$ )
			706 m,n	
	1060 S,vb		1060 s,vb	CoO (overtone?)

Abbreviations: b, broad; m, medium; n, narrow; S, strong; v, very; w, weak.

pure reagent at 2920 to 2853  $\text{cm}^{-1}$  to the graft of surfactants on the cobalt surface.<sup>39</sup> Furthermore, the peaks attributed to the stretching mode of the carboxylic group at 1711 and 1285  $\text{cm}^{-1}$  are absent in the spectrum of the coated cobalt NPs. Instead, two new bands at 1563 and 1415  $\text{cm}^{-1}$ , characteristics of the asymmetric and symmetric COO–stretch, respectively, appear. From these results, a chemical bond between O and Co atoms around the NP surface was deduced.<sup>39</sup> In our case, the wavenumber of  $\nu\text{CH}_n$  remains constant that indicates a weaker coupling between metal and ligands. It is likely that the use of KBr matrix modifies the local chemistry.

A significant absorption is observed for the film of cobalt NPs, the maximum of which is at 1556  $\text{cm}^{-1}$ . The presence of metal particles modifies the interaction with light and the optical spectrum is mainly a reflection spectrum as conventionally observed in the infrared analysis

of a metal or a combination of absorption and reflection components.<sup>73,74</sup> In the first case, the wavenumber to consider is that of the inflection point, which is measured at  $\sim 1630 \text{ cm}^{-1}$ . A second, more intense reflection band is also observed at  $\sim 1450 \text{ cm}^{-1}$  associated with a peak at 1390  $\text{cm}^{-1}$ . The two measurement methods have significant weaknesses; the dispersion in KBr promotes the reaction between the compounds, while the NP film analysis maximizes the reflection components. The observation of different components is consistent with the formation of bi-dentate carboxylate bond.

New and intense infrared bands are observed at lower wavenumbers: 798, 1020, and 1093 and 1261  $\text{cm}^{-1}$  for the film of partially “oxidized” cobalt NPs. The triplet at 1410, 1431, and 1461  $\text{cm}^{-1}$  ( $\text{CH}_2$  bending) observed in the acid, not observed for Co metal NPs, becomes again visible but is weaker (Figure 4A and Table 1). The high



residual intensity of these bands is to be linked to the very polar nature of these bonds favoring the infrared intensity, in particular of the modes involving the C–O group. Therefore, one can say that, in the coated NPs, the intensity of C=O stretching mode strongly decreases because the lauric acid is chemisorbed as a carboxylate onto the NP surface.

### 3.4.2 | Raman signatures

The easy observation of the signature of the organic ligands (and we will see it later of the oxidized layer on the surface of the cobalt NPs) despite the very small thickness is explained by a resonant character of the Raman spectrum. The Raman spectrum of the ligand is stronger when the NPs are deposited on an HOPG wafer (and we will only discuss these results; Figure 4B). One advantage of this substrate is its very good capacity to conduct heat and hence to avoid local heating, which would damage the NP assembly. Indeed, the Raman spectrum appears extremely sensitive to the illumination laser power: Under 50  $\mu\text{W}$ —a very low illumination power, the number of Raman peaks is limited and their wavenumber is very similar or identical to those measured for the acid.

A moderate increase in power induces a new band to arrive at  $1582\text{ cm}^{-1}$  and increases the intensity of the band to  $2727\text{ cm}^{-1}$ , both modes being characteristic of the fundamental and overtone mode of C–C HOPG substrate.<sup>51,75</sup> The quasi absence of HOPG signature for pristine Co@shell NP film evidences the complete coverage by NPs in the studied area. The increase of the intensity of HOPG with laser intensity can be explained by the reduction in thickness or even the formation of holes in the NP film, so that the contribution of the HOPG substrate becomes more and more significant. We also observe the appearance of the thin peak at  $3248\text{ cm}^{-1}$  and the wider band at  $2440\text{ cm}^{-1}$ . The rest of the spectrum is hardly changed, except for a small widening of the C–H elongation modes visible by the poorer identification of the modes appearing as shoulders. Long-term exposure (a few tens of minutes) leads to the degradation of the surface of the HOPG substrate (broadening of the carbon modes) with retention of the signature of cobalt oxide.

The main difference with spectrum of lauric acid<sup>76–79</sup> is the appearance of a broad band around  $535\text{ cm}^{-1}$ . This broadness is consistent with the signature of an inorganic metal oxide phase, the shell.

The observation of the bands characteristic of ligands indicated that lauric acid, similar to pure Co NPs, serves as a ligand providing stability. The role of the ligand must

be emphasized here: As demonstrated by Kazmierczak et al.,<sup>80</sup> the carboxylate group interacts by bridging the  $\text{Co}^{2+}$  ions on the particle surface, which not only effectively protects against coalescence and ensures colloidal stability but also protects against oxidation, which explains the time required to obtain the oxide shell (12 days).

### 3.5 | Raman characterization of the “oxidized” shell under different laser wavelength

Figure 5 compares the Raman spectra of an NP film of “oxidized” cobalt NPs to that of the oxides CoO (rock salt structure) and  $\text{Co}_3\text{O}_4$  (spinel structure) in their powder form<sup>81–83</sup> deposited on a gilded glass plate. These powders are strongly colored and hence very sensitive to local heating under laser spot. Spectra of Figure 5 have been

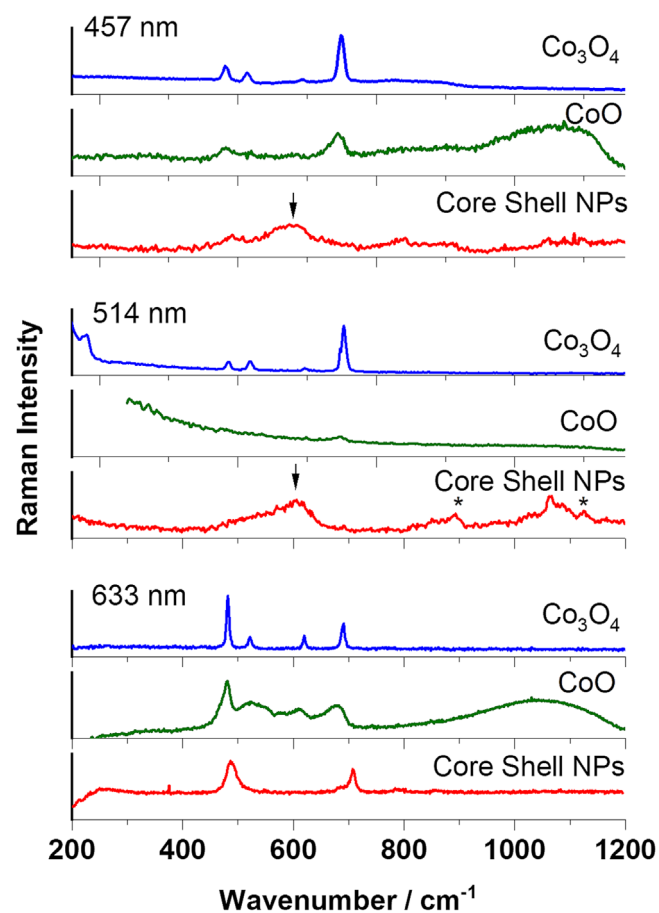


**FIGURE 5** Comparison of the Raman spectra recorded under different laser excitations, red (632 nm,  $100\times$ ,  $100\ \mu\text{W}$ ), green (514 nm,  $200\times$ ,  $100\ \text{cc}\mu\text{W}$ ), and blue (457 nm,  $200\times$ ,  $100\ \mu\text{W}$ ) for partially oxidized (core shell) nanoparticles (NP) and cobalt oxide references ( $\text{Co}_3\text{O}_4$  and CoO in their powder form); asterisks (\*) indicate ligand modes.

recorded under 100  $\mu\text{W}$  laser power (at the sample) that corresponds empirically to a power of illumination sufficiently low to prevent phase modification. We will first consider the spectra of reference powders recorded under green laser excitation.

### 3.5.1 | Cobalt oxide powder reference

Due to the rock salt symmetry, no fundamental mode is expected—and observed—for CoO in Raman spectroscopy (a 510  $\text{cm}^{-1}$  mode is observed in infrared).<sup>81</sup> However, the study of nanometric cobalt oxide by Rivas-Mirias et al.<sup>82</sup> shows an asymmetric mode at 530  $\text{cm}^{-1}$  and a minor band at 680  $\text{cm}^{-1}$  in addition to the second-order mode at 1060  $\text{cm}^{-1}$ . The 530  $\text{cm}^{-1}$  band corresponds to the longitudinal optic mode measured in infrared. Previous work reported, as on our spectrum, the contamination by the signature of the spinel phase ( $\text{Co}_3\text{O}_4$ ) at  $\sim 200$ , 480, and 680  $\text{cm}^{-1}$ <sup>81–83</sup>, in particular if the laser power is increased. Indeed, we observe a very weak signal corresponding to the main peak of  $\text{Co}_3\text{O}_4$  phase. This confirms the poor stability of CoO oxide under laser beam.

The Raman spectrum of the  $\text{Co}_3\text{O}_4$  spinel recorded with blue laser shows all the expected modes, at 195 ( $F_{2g}$ ), 480 ( $E_g$ ), 515 ( $F_{2g}$ ), 615 ( $F_{2g}$ ), and the most intense at 685  $\text{cm}^{-1}$  ( $A_{1g}$ ).<sup>81–83</sup> Due to the largest deformation of the electronic cloud involved with stretching  $A_1$  metal-oxygen atom mode, this mode is the stronger of the Raman spectrum. The vibration modes of spinel structure are strongly coupled (oxygen atoms belong to both tetrahedron and octahedron) but it is common to consider of the  $\sim 685$   $\text{cm}^{-1}$  mode as octahedron stretching.<sup>81–84</sup> Our spectra obtained with the excitations at 457 and 514 nm show traces of  $\text{Co}_3\text{O}_4$  in the CoO compound and the second-order component according to Raman resonance effect. The 530  $\text{cm}^{-1}$  band is possible while not very visible. According to the strong coloration of the oxides, the resonance effect induces small wavenumber shift and relative intensity changes with exciting wavelength. This study of reference powder shows the huge sensitivity of cobalt oxide toward laser illumination, even at a power lower than usually used for inorganic samples. Moreover, the high absorption of the powders also implies a high absorption of the scattered Raman photons, making the Raman signal particularly weak.

### 3.5.2 | NPs assembly

The spectrum obtained for the NP films of partially oxidized cobalt NPs under 457 and 514 nm laser lines shows

a main band at 608  $\text{cm}^{-1}$  (full width at half height: 43  $\text{cm}^{-1}$ ) and a lower one at 497  $\text{cm}^{-1}$  (full width at half height: 87  $\text{cm}^{-1}$ ). The spectrum is therefore different from that reported for nanometric CoO and of course for  $\text{Co}_3\text{O}_4$ . The phase is therefore different and more disordered. Obviously, spectrum recorded under red laser looks more crystalline (width: 10  $\text{cm}^{-1}$ ) due to a structure modification under the laser beam, according the “strong” light absorption at 632 nm (Figure 3).

The spectrum at 514 nm also shows features due to the organic molecules. These peaks are not noticed in Table 2 and are marked with an asterisk in Figure 5.

The spectrum recorded under red laser shows the presence of oxide layer, but at least (partially?) transformed under laser beam into  $\text{Co}_3\text{O}_4$  and perhaps with a more complete oxidation of the core of Co NPs. This is consistent with the UV-visible absorption curves of Figure 3 that shows that all laser lines are located at wavelength absorbed by the electronic transition. Absorbance being stronger in red range, obviously, the heating effect will be maximal under 633 nm analysis. As evidence, no peaks characteristic of the ligands is observed. Spectra recorded under green and blue excitation are different. They do not correspond to CoO or  $\text{Co}_3\text{O}_4$  phases. The closest spectrum is that of delafossite (formula expressed as  $\text{HCoO}_2$  or  $\text{CoOOH}$ ), a variety of natural heterogenite<sup>85–88</sup> which shows an intense peak at  $\sim 500$   $\text{cm}^{-1}$  (we observe it at 497  $\text{cm}^{-1}$ ) and a broad component around 620  $\text{cm}^{-1}$  (we observe it at 608  $\text{cm}^{-1}$ ). The layered structure of delafossite is consistent with the formation of a very thin oxide layer (Co–O bond length equal about 0.2 nm, and hence, the shell consists of two to three Co–O bonds).

## 3.6 | Dynamics in the heated film

Increasing the laser illumination power above  $\sim 1$  mW shows a broadening and intensity decrease of the Raman signal (Figure 4B). Examination of the materials with an optical microscope shows a loss of the focus: It is no longer possible to obtain a sharp image, indicating a dynamic disorder of the NP assembly (Figure S2). This led us to study the NP assembly at different temperatures in a heating cell. Figure 6 compares the evolution of the spectrum of the cobalt NP film with increasing temperatures, in the range of very low wavenumbers (Lamb modes; Figure 6A) and  $\nu\text{C-H}$  (ligands) and  $\nu\text{C-C}$  (HOPG substrate) modes (Figure 6B). We observe the disappearance of the mode at  $\sim 10$   $\text{cm}^{-1}$  that merges with the Rayleigh wing and the increase in the intensity of the ro-vibrational components of the  $\text{N}_2$  molecules in the air.<sup>89,90</sup> The increase in  $\text{N}_2$  peaks is explained by the

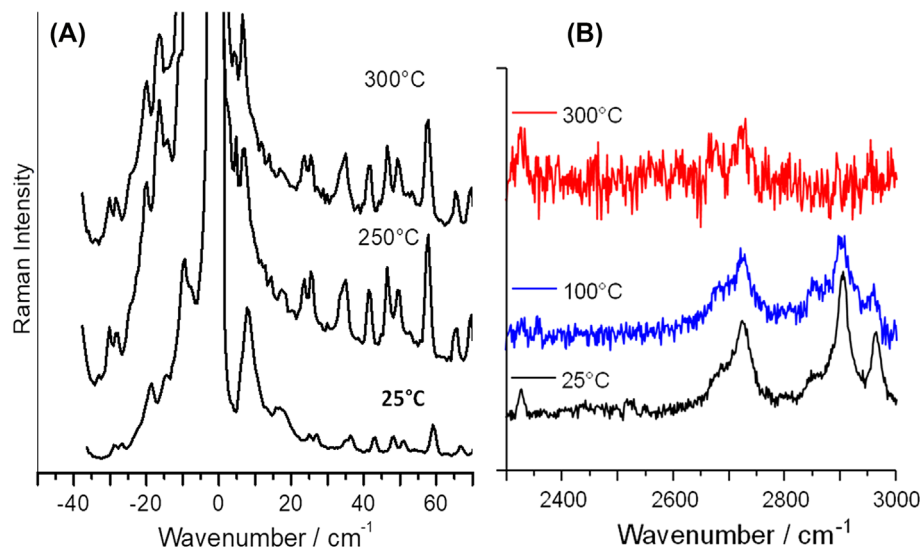


**FIGURE 6** Spectra recorded at different temperatures in heating cell: (A) anti-Stokes and Stokes low-wavenumber range and (B) spectral range of the C–C bond HOPG overtones.

existence of multireflection of light between metal surfaces, which, by increasing the optical path, makes the signal more intense. Their observation is common when the volume probed promotes local multiple reflections of the laser beam at reflective interfaces (e.g. bubbles and metal surface).<sup>91</sup> The component of the HOPG substrate at  $2730\text{ cm}^{-1}$  becomes dominant. The formation of a Rayleigh wing indicates strong disorder, static and/or dynamic.

The increase of the length path makes the signature of the gas phase significant. The observation of  $\text{N}_2$  ro-vibrational mode (narrow peaks before and above the main  $\sim 60\text{ cm}^{-1}$  peak) suggests that the oxide shell is degraded. These changes of the spectroscopic signature are consistent with a destruction of the NP assembly with likely some desquamation of the shell from the metal core.

## 4 | CONCLUSION

A multiscale analysis of pure and core-shell cobalt NPs was performed. The cobalt NPs remain stable at intermediate temperatures and we evidenced the progressive degradation of the coatings at temperatures above  $100^\circ\text{C}$  which correlates with the loss of topological order evidenced with the strong Rayleigh wing observed.

The formation of the oxide shell previously detected by TEM is clearly demonstrated by the change in the optical signature regardless of the technique used, UV–visible–NIR absorption, infrared transmission, and Raman spectroscopy before and after oxidation. The agreement between analyses on very different volumes, from the nanometric scale (TEM) to the scale of several

square micrometers (Raman) and macroscopic (FTIR and UV–visible–NIR), indicates good homogeneity of the products. Hydroxylation or water adsorption is observed for the Co film.


It is clear that the shell formed by oxidation is neither  $\text{CoO}$  nor  $\text{Co}_3\text{O}_4$  but amorphous with a structure and composition close to  $\text{CoOOH}$  (delafossite).<sup>87,88</sup> This protonation is consistent with the “consumption” of water molecules encapsulated in the ligands of the cobalt NPs or dangling OH bonds at the surface of the metallic NPs observed by FTIR spectroscopy before the oxidation treatment. It should be recalled that the protonation of the oxide layers is associated with the network stabilization and healing of electrical defects resulting from the curvature of the structure, as observed in asbestos.<sup>92–94</sup> The structure of delafossite potentially opens the way to numerous properties that can enhance surface reactivity: adsorption and ion exchange and catalytic or electrochemical properties.

## ORCID

Ghilhem Simon  <https://orcid.org/0000-0002-7824-561X>

Salvatore Costanzo  <https://orcid.org/0000-0001-9236-0393>

Isabelle Lisiecki  <https://orcid.org/0000-0001-7764-3125>

Philippe Colombar  <https://orcid.org/0000-0001-6099-5423>

## REFERENCES

- [1] E. Matijevic, *Langmuir* **1986**, *2*, 12.
- [2] P. Colombar, *Ceram. Int.* **1989**, *15*, 23.
- [3] P. Colombar, *Ceramics Switzerland* **2020**, *3*, 312.
- [4] R. Kesavamoorthy, S. Tandon, S. Xu, S. Jagannathan, S. A. Asher, *J. Colloid Interface Sci.* **1992**, *153*, 188.

- [5] M. P. Pileni, *Langmuir* **1997**, *13*, 3266.
- [6] P. Zhao, N. Li, D. Astruc, *Coord. Chem. Rev.* **2013**, *257*, 638.
- [7] J. H. Fendler, F. C. Meldrum, *Adv. Mater.* **1995**, *7*, 607.
- [8] M. Rycenga, C. M. Cobley, J. Zeng, W. Li, C. H. Moran, Q. Zhang, D. Qin, Y. Xia, *Chem. Rev.* **2011**, *111*, 3669.
- [9] C. Petit, A. Taleb, M. P. Pileni, *Adv. Mater.* **1998**, *10*, 259.
- [10] V. F. Puntès, K. M. Krishnan, A. P. Alivisatos, *Top. Catal.* **2002**, *19*, 145.
- [11] A. H. Lu, E. L. Sabalas, F. Schüth, *Angew. Chem. Int. Ed.* **2007**, *46*, 1222.
- [12] I. Lisiecki, M. P. Pileni, *Langmuir* **2003**, *19*, 9486.
- [13] S. W. Charles, *J. Magn. & Magnet Mater* **1987**, *65*, 350.
- [14] B. Slibeiki, P. Kameli, H. Salamati, G. Concas, F. M. Fernandez, A. Talone, G. Muscas, D. Peddis, *Belstein J. Nanotechn.* **2019**, *10*, 856.
- [15] R. K. Ramamoorthy, A. Viola, B. Grindi, J. Peron, C. Gatel, M. Hytch, R. Avenal, L. Sicard, M. Giraud, J. Y. Piquemal, G. Viau, *Nano* **2019**, *19*, 9160.
- [16] M. Grzelczak, J. Vermant, E. M. Furst, L. M. Liz-Marzan, *ACS Nano* **2010**, *4*, 3591.
- [17] M. J. Hajipour, K. M. Fromm, A. A. Ashkarran, *Trends Biotechnol.* **2012**, *30*, 4999.
- [18] Z. Nie, A. Petukhova, E. Kumacheva, *Nature Nanotechnol* **2010**, *5*, 15.
- [19] P. Bharadwaj, B. Deutsch, L. Novotny, *Adv Opt & Photon* **2009**, *1*, 438.
- [20] C. Loo, A. Lin, L. Hirsch, *Technol. Cancer Res. Treat.* **2004**, *3*, 33.
- [21] S. Guo, S. Zhang, S. Sun, *Angew. Chem. Int. Ed.* **2013**, *52*, 8526.
- [22] J. F. Li, Y. J. Zhang, S. Y. Ding, R. Panneerselvam, Z. Q. Tian, *Chem. Rev.* **2017**, *117*, 5002.
- [23] A. Walcarius, *Chem. Soc. Rev.* **2013**, *42*, 4098.
- [24] L. Fan, S. Y. Wei, S. Y. Li, Q. Li, Y. Y. Lu, *Adv Energ Mater* **2018**, *8*, 1702657.
- [25] A. Coskun, J. M. Spruell, G. Barin, W. R. Dichtel, A. H. Flood, Y. Y. Botros, J. F. Soddart, *Chem. Soc. Rev.* **2012**, *41*, 4827.
- [26] L. Rassaei, M. Amiri, M. Ciprian, M. Sillanpaa, F. Marken, M. Sillanpaa, *TRAC-Trends Anal. Chem.* **2011**, *30*, 1704.
- [27] J. T. Cox, B. Zhang, *Annu. Rev. Anal. Chem.* **2012**, *5*, 253.
- [28] Y. Pan, W. J. Paschoalino, A. S. Blum, J. Mauzeroll, *ChemSusChem* **2021**, *14*, 758.
- [29] X. Y. Li, Y. M. Chen, H. T. Huang, Y. W. Mai, L. M. Zhou, *Energy Storage Mater* **2016**, *5*, 58.
- [30] N. Wu, L. Fu, M. Aslam, K. C. Wong, V. P. Dravid, *Nano Lett.* **2004**, *4*, 383.
- [31] T. Xiang, J. Zong, W. Xu, Y. Feng, H. Chen, *Mater. Chem. Front.* **2021**, *5*, 465.
- [32] S. M. Ansari, R. D. Bohr, K. R. Pai, D. Shen, S. Mazumder, K. Ghosh, Y. D. Kolekar, *Appl. Surf. Sci.* **2017**, *414*, 171.
- [33] C. Hanske, M. N. Sanz-Ortiz, L. M. Liz-Marzan, *Adv. Mater.* **2018**, *30*, 1707003.
- [34] J. Krajczewski, H. B. Abdulrahman, K. Kolataj, A. Kudelski, *Spectrochim Acta Part A-Mol. & Biomol Spectrosc* **2018**, *193*, 480.
- [35] G. Gouadec, P. Colomban, *J. Raman Spectrosc* **2007**, *38*, 598.
- [36] V. Sepelak, K. D. Becker, I. Bergmann, S. Suzuki, S. Indris, A. Feldhoff, P. Heitjans, C. P. Grey, *Chem. Mater.* **2009**, *21*, 2518.
- [37] A. H. Latham, M. E. Williams, *Langmuir* **2008**, *24*, 14195.
- [38] P. Roonasi, A. Holmgren, *Surface* **2009**, *255*, 5891.
- [39] A. Ledo-Suarez, L. Rodriguez-Sanchez, M. C. Blanco, M. A. Lopez-Quintela, *Phys Stat Solidi –ApplMater Sci* **2006**, *203*, 1234.
- [40] C. R. K. Rao, D. C. Trivedi, *Synth. Met.* **2005**, *155*, 324.
- [41] H. Yang, Y. Wang, H. Huang, L. Gell, L. Lehtovaara, S. Malola, H. Hakkinen, N. Zheng, *Nature Comm* **2013**, *4*, 2422.
- [42] N. Goubet, J. Richardi, P. A. Albouy, M. P. Pileni, *J. Phys. Chem. Lett.* **2011**, *2*, 417.
- [43] L. Robinet, M. C. Corbeil, *Stud Conserv* **2003**, *48*, 23.
- [44] Y. F. Wang, A. Neyman, E. Arkhangelsky, V. Gitis, L. Meshi, I. A. Weinstok, *J. Am. Chem. Soc.* **2009**, *131*, 17412.
- [45] M. P. Pileni, *J. Colloid Interface Sci.* **2012**, *388*, 1.
- [46] A. Cazacu, C. Larosa, P. Beaunier, G. Laurent, P. Nanni, L. Mitoseriu, I. Lisiecki, *Adv. Funct. Mater.* **2014**, *24*, 164.
- [47] G. Bahmanrokh, M. Hashim, I. Ismail, N. Soltani, P. Vaziri, M. Shamsul, E. Shafie, M. Navaseri, *J. Supercond. Novel Magn.* **2013**, *26*, 407.
- [48] C. Salzemann, V. Russier, M. Pancaldi, P. Vavassori, P. Berger, I. Lisiecki, *Colloids Surf., a* **2023**, *678*, 132473.
- [49] E. Duval, *Phys. Rev. B* **1992**, *46*, 5795.
- [50] E. Duval, L. Saviot, A. Mermet, D. B. Murray, *J. Phys. Condens. Matter* **2005**, *17*, 3559.
- [51] G. Gouadec, P. Colomban, *Prog. Cryst. Growth Charact. Mater.* **2007**, *53*, 1.
- [52] I. Lisiecki, D. Polli, C. Yan, G. Soavi, E. Duval, G. Cerulla, M. P. Pileni, *Nano Lett.* **2013**, *13*, 4914.
- [53] G. Simon, L. Meziane, A. Courty, P. Colomban, I. Lisiecki, *J Raman Spectrosc* **2016**, *47*, 248.
- [54] J. Creighton, C. Blatchford, M. Albrecht, *J. Chem. Soc. Faraday Trans.* **1979**, *75*, 790.
- [55] M. Fleischmann, P. J. Hendra, A. J. Mcquillan, *Chem. Phys. Lett.* **1974**, *26*, 163.
- [56] D. L. Jeanmaire, R. P. Van Duyne, *J. Electroanal. Chem.* **1977**, *84*, 1.
- [57] I. Kosacki, T. Suzuki, H. Anderson, *Solid State Ion.* **2002**, *149*, 99.
- [58] M. Ivanda, K. Furić, S. Musić, M. Ristić, M. Gotić, D. Ristić, A. M. Tonejc, I. Djerdj, M. Mattarelli, M. Montagna, F. Rossi, M. Ferrari, A. Chiasera, Y. Jestin, G. C. Righini, W. Kiefer, R. R. Gonçalves, *J Raman Spectrosc* **2007**, *38*, 647.
- [59] A. Andrieux-Ledier, B. Tremblay, A. Courty, *J. Phys. Chem. C* **2013**, *117*, 14850.
- [60] M. A. Ben Aissa, B. Tremblay, A. Andrieux-Ledier, E. Maisonhaute, N. Rouafi, A. Courty, *Nanoscale* **2015**, *7*, 3189.
- [61] Y. J. Zhang, Q. Q. Chen, X. Chen, A. Wang, Z. Q. Tian, J. F. Li, *J Raman Spectrosc* **2021**, *52*, 439.
- [62] T. J. Li, B. Y. Wen, Y. J. Zhang, L. Zhang, J. F. Li, *J Raman Spectrosc* **2022**, *53*, 1386.
- [63] H. Aghdam, S. Dizajghorbani, S. Moemen Bellah, R. Malekfar, *Spectrochim. Acta Part a: Mol & Biomol Spectrosc* **2019**, *223*, 117379.
- [64] I. Lisiecki, P. A. Albouy, M. P. Pileni, *Adv. Mater.* **2003**, *15*, 712.
- [65] I. Lisiecki, P. A. Albouy, M. P. Pileni, *J. Phys. Chem. B* **2004**, *108*, 20050.
- [66] S. Costanzo, G. Simon, P. Colomban, I. Liesieki, *J. Phys. Chem. C* **2016**, *120*, 22054.
- [67] T. Buffeteau, D. De Sousa Meneses, M. Dussauze, T. Tassaing, *Spectroscopie infrarouge*, in *Spectroscopies Vibratoires*:

- Théorie, aspects pratiques et applications*, (Ed: G. Simon), Editions des archives contemporaines, Paris, France **2020** 47.
- [68] L. F. Vieira Ferreira, I. Ferreira Machado, A. M. Ferraria, T. M. Casimiro, P. Colomban, *Appl Surf Sci Part B* **2013**, 285, 144.
- [69] D. Visinescu, C. Paraschiv, A. Ianculescu, B. Jurca, B. Vasile, O. Carp, *Dyes & Pigments* **2010**, 87, 125.
- [70] J. Shim, C. Venkata Reddy, G. V. S. S. Sarma, P. Narayana Murthy, R. V. S. S. N. Ravikumar, *Spectrochim. Acta Part A-Mol. Biomol Spectrosc.* **2015**, 142, 279.
- [71] M. B. Kime, D. Makgoale, *Chem. Engn Comm.* **2016**, 203, 1648.
- [72] P. Colomban (Ed), *Proton Conductors*, Cambridge University Press, Cambridge, UK **1992**.
- [73] P. Colomban, A. Gruger, A. Novak, A. Régis, *J. Mol. Struct.* **1994**, 317, 261.
- [74] P. Colomban, A. Gruger, A. Régis, *C-R Acad Sci Paris* **1995**, 321-série IIB, 247.
- [75] P. H. Tan, S. Dimovski, Y. Gogotsi, *Phil Trans R Soc Lond a* **2004**, 362, 2289.
- [76] I. R. Hill, I. W. Levin, *J. Chem. Phys.* **1979**, 70, 842.
- [77] P. D. Moran, G. A. Bowmaker, R. P. Cooney, J. R. Barlett, J. L. Woolfrey, *J. Mater. Chem.* **1995**, 5, 295.
- [78] V. Otero, D. Sanches, C. Montagner, M. Vilarigues, L. Carlyle, J. A. Lopes, M. J. Melo, *J Raman Spectrosc* **2014**, 45, 1197.
- [79] S. M. Baqer Albahrani, G. Simon, S. Ayrinhac, M. Gauthier, F. Decremps, I. Lisiecki, S. Costanzo, P. Colomban, *Eur. Phys. J. B.* **2019**, 92, 35.
- [80] K. Kazmierczak, D. Yi, A. Jaud, P. F. Fazzini, M. Estrader, G. Viau, P. Decorse, J. Y. Piquemal, C. Michel, M. Besson, K. Soulantica, N. Perret, *J. Phys. Chem. C* **2021**, 125, 7711.
- [81] W. L. Qiu, F. Qin, H. Fan, V. G. Fang, Y. Hadjiev, D. Li, J. B. Litvinov, *J. Phys. Chem.* **2016**, 120, 4511.
- [82] B. Rivas-Murias, V. Salgueirino, *J Raman Spectrosc* **2017**, 48, 837.
- [83] S. Farhadi, J. Safabakhsh, *J Alloys Compnds* **2012**, 515, 180.
- [84] Z. Cvejic, S. Rakic, A. Kremenovic, B. Antic, C. Jovalekic, P. Colomban, *Solid State Sci.* **2006**, 8, 908.
- [85] D. Upadhyay, B. Roondhe, A. Pratap, P. K. Jha, *Appl. Surf. Sci.* **2019**, 476, 198.
- [86] C. Burlet, H. Goethals, Y. Vanbrabant, *Spectrochim Acta Part a: Mol. Biomol Spectrosc* **2016**, 159, 90.
- [87] M. A. Marquardt, N. A. Ashmore, D. P. Cann, *Thin Solid Films* **2006**, 496, 146.
- [88] F. Podjaski, D. Weber, S. Zhang, L. Diehl, R. Eger, V. Duppel, B. V. Lotsch, *Nat. Catal.* **2020**, 3, 55.
- [89] H. Okajima, H. Hamaguchi, *J Raman Spectrosc* **2015**, 46, 1140.
- [90] A. Raj, C. Kato, H. A. Witek, H. Hamaguchi, *J Raman Spectrosc* **2020**, 51, 2066.
- [91] P. Colomban, J. M. Herrera Ramirez, R. Paquin, A. Marcellan, A. Bunsell, *Engn Fract. Mech.* **2006**, 73, 2463.
- [92] E. J. W. Whittaker, Structure and Properties of Asbestos, in *Handbook of Textile Fibre Structure*, Woodhead Publishing, Sawston, UK **2009** 425.
- [93] L. Bonneau, H. Suquet, C. Malard, H. Pezerat, *Environ. Res.* **1986**, 41, 251.
- [94] A. M. Langer, M. S. Wolff, A. N. Rohl, I. J. Selikoff, *J Toxicol Environm Health Part a Current Issues* **1978**, 4, 173.

## SUPPORTING INFORMATION

Additional supporting information can be found online in the Supporting Information section at the end of this article.

**How to cite this article:** G. Simon, S. Costanzo, I. Lisiecki, P. Colomban, *J Raman Spectrosc* **2024**, 1. <https://doi.org/10.1002/jrs.6668>